Prediction of stochastic behavior in differential charging of nanopatterned dielectric surfaces during plasma processing

Jason A. Kenney and Gyeong S. Hwang[a)]
Department of Chemical Engineering, The University of Texas, Austin, Texas 78712

(Received 17 August 2006; accepted 27 November 2006; published online 23 February 2007)

We investigate differential charging of high aspect ratio dielectric trenches under plasma exposure using a two-dimensional computational model. Rather than considering average fluxes, we track individual ion and electron trajectories within the electric field arising from surface charges on the trench, updating the potentials within the computational domain after each particle. Our results show that, as the trench width shrinks to 100 nm and below, the potentials within the trench oscillate over an ever-wider range. The stochastic charging behavior in turn leads to noticeable changes in the flux and energies of ions passing through the trench. © *2007 American Institute of Physics*.
[DOI: 10.1063/1.2433134]

I. INTRODUCTION

Differential surface charging of insulating or partially conducting materials is commonly caused by unbalanced fluxes between oppositely charged impinging species and/or inhomogeneities in surface electrical properties. The precise determination of the rate and asymmetry of surface charging has been an issue of great importance in a range of scientific and technological areas, such as x-ray photoelectron spectroscopic measurements,[1] dusty plasma studies,[2,3] spacecraft design and operation,[4] and microelectronic device fabrication.[5–7] In particular, differential charging is often a serious drawback in applying plasma processing technology to define high aspect ratio structures in the manufacture of modern microelectronic and photonic devices and micro- and nanoelectrochemical systems. Moreover charging-induced discharges can significantly affect product yields.

It is well established that charges can accumulate on the exposed insulating surfaces of patterned structures during plasma etching and deposition, due to the directionality differences between impinging ions and electrons. This, in turn, gives rise to electric fields which can alter the trajectory, flux, and kinetic energy of incident ions, often resulting in undesirable side effects in the plasma-assisted processes. Many theoretical studies[8–12] have been undertaken to elucidate this charging behavior and how ion and electron trajectories are modified by electric fields, in terms of plasma conditions, surface topologies, and surface electrical properties. In most of these earlier studies, charge accumulation and potential distribution were updated on set intervals using average fluxes of the impinging species. This approach may be suitable for finding the mean behavior of surface charge densities and potential distributions when the dimension of patterned structures is sufficiently large. However, as device feature sizes shrink into the nanometer scale regime, the influence of an individual charge transferred to the surface will be larger, leading to an increase in the variability of potentials within the charging area. This leads to the question of whether a true steady-state-like behavior will be reached for high aspect ratio dielectric structures with a small absolute dimension or will large oscillations in the potential lead to essentially stochastic behavior.

In this study, we investigate this variability and look for an evidence of stochastic behavior. We consider individual ion and electron species impinging on high aspect ratio dielectric structures of varying absolute dimension, with charge transfer and updates to the potential occurring after each impact with the dielectric. We illustrate the variation of the potential in the structure with dimension and show how the potential evolves and fluctuates at the exit of the structure. Finally, we demonstrate the effect of the above on the flux and energies of ions exiting the domain as compared with those of entering ions. This work represents a theoretical effort to determine the effect of pattern dimensions on surface charging behavior during plasma processing. The improved understanding will assist in explaining and predicting the complex behavior of surface charging and feature profile evolution in application of plasma techniques to the fabrication of future nanostructure-based devices.

II. SIMULATION METHODS

As depicted in Fig. 1, our charging simulations were performed on a two-dimensional dielectric trench structure with an aspect ratio of 5 and an open bottom. The trench width is varied from 500 to 100 to 50 nm. In each case, the width of the simulation domain is three times the trench width, and the upper/lower boundary plane is located four times the trench width above/below the trench structure. The open bottom structure was chosen as a convenient means to demonstrate stochastic charging behavior. In real plasma-based processing of semiconductor devices, however, the trench bottom would be closed, with either a conducting or an insulating material. This may in turn alter to a certain degree the charging behavior under investigation.

Our simulation strategy, as depicted in the flowchart in Fig. 2, is as follows: (1) generate an ion or electron by sampling from a given energy distribution function and randomly determining a position at the upper boundary plane; (2) track

[a)]Author to whom correspondence should be addressed; electronic mail: gshwang@che.utexas.edu

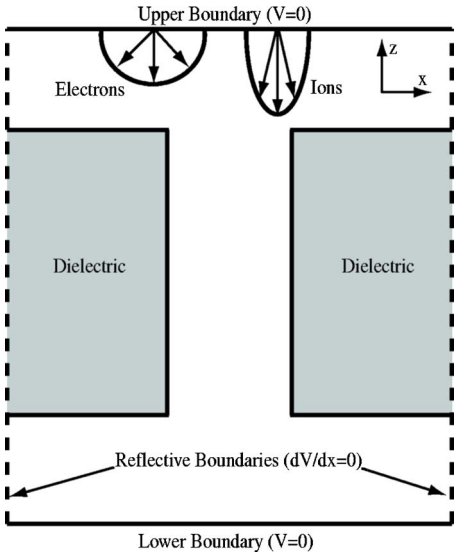

FIG. 1. (Color online) Schematic of the simulation domain (not to scale).

the motion of the generated species in the electric field arising from the differential charging of the trench; (3) transfer the charge of the species to the dielectric structure in the event of a collision; and (4) update the potential and electric fields after each collision. Ions which travel through the structure without colliding are tracked until they reach the lower boundary plane, and their energies are recorded. At set intervals (described below), the conduction of charge along the surface is calculated and the potential and electric fields are updated.

In order to generate ions and electrons, we assume a flux of 1.0×10^{16} cm^{-2} s^{-1} for each species,[13] giving an equal probability for randomly choosing the next particle type. For the electrons, an average temperature of 4 eV is used for the Boltzmann distribution from which x and z velocities are obtained. Similarly, ions (assumed to be Ar^+) are assumed to have an average temperature of 300 K in order to generate thermal x and z velocities. To the thermal z component, a directed z velocity is added, sampled from a bimodal energy distribution (details below). For all of the above, pseudorandom numbers are generated using a Mersenne Twister algorithm.[14]

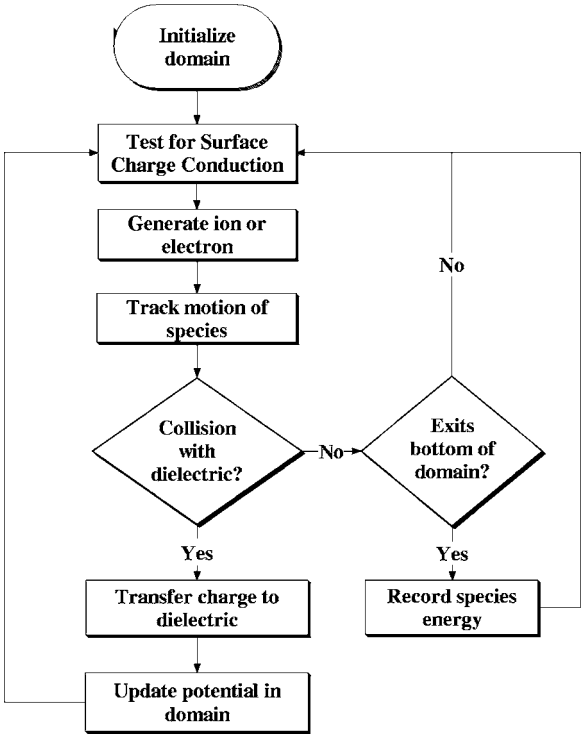

FIG. 2. Flowchart of the computational structure.

The potential distribution in the vacuum regime is calculated with the Laplace equation ($\nabla^2 V=0$). Gauss's law ($\mathbf{n}\cdot\nabla V=-\sigma/\varepsilon_0$) is used at locations adjacent to the dielectric surface, where $\mathbf{n}$ is the outward normal, σ is the surface charge density, and ε_0 is the permittivity of free space. The conjugate gradient method is employed to update the potential upon each collision of a particle with the dielectric surface or during the calculation of the surface conduction. The upper and lower boundaries in the simulation domain have the potential set to zero. Reflective boundary conditions are used at domain side boundaries. The simulation domain is divided into small square meshes: In x and z dimensions, the mesh length is one-eighth of the trench width, and a y dimension is assumed equal to one x-/z-mesh length where necessary.

Tracking the motion of the charged particles in the electric field is accomplished through the use of the equation of motion for each particle, following the treatment of Birtles[15] and considering the electric fields within the domain as fixed during the particle motion. The fourth-order Runge-Kutta method is employed, with a time step chosen to ensure that the particle does not travel more than one-fourth of a mesh length in any dimension. The electric field is calculated at mesh points using finite differences on the potentials. The field local to the particle is then given by an equation of the following form:

$$\mathbf{E}=(1-\bar{x})(1-\bar{z})\mathbf{E}_{0,0}+(\bar{x})(1-\bar{z})\mathbf{E}_{1,0}+(1-\bar{x})(\bar{z})\mathbf{E}_{0,1}+(\bar{x})(\bar{z})\mathbf{E}_{1,1}, \quad (1)$$

where $\mathbf{E}_{x,z}$ are the electric field vectors at corners of the cell containing the particle and $\bar{x}$ and $\bar{z}$ are the relative positions of the particle within the cell, normalized by the x- and z-mesh lengths, respectively.

We assume a sheet resistance of 1×10^{20} Ω, which falls at the high end of experimentally reported values for SiO_2.[16] The calculation of surface conduction is accomplished by an explicit scheme: (1) The potentials of nodes on the dielectric surface are compared to their neighbors; (2) currents into and out of the nodes are determined based on these potential differences and surface resistances between nodes; (3) charge transfers are calculated for a specified time step; and (4) all potentials within the domain are recalculated. As the time scales of the surface conduction and that of ions and electrons entering the domain differ, the surface conduction is not calculated after every particle. Rather, we choose a time step for the surface conduction such that approximately one-tenth of the charge differential is transferred between nodes before updating all potentials within the domain. The time step is dependent on the mesh sizes used and is given by

$$\Delta t_{\text{conduction}} = 0.1 R_S \varepsilon_0 \min\left(\frac{x^2}{z}, \frac{z^2}{x}\right), \tag{2}$$

where R_S is the sheet resistance and x and z are the mesh lengths in the x and z dimensions. For the sheet resistance and mesh sizes used here, this value ranges from ~0.5 to ~5 s, which is 10^5–10^8 times as large as the respective time per particle. With this same scheme, consideration of a sheet resistance of 1×10^{16} Ω (the lower end of the experimentally reported range) would give much smaller ratios of 10^1–10^4 relative to the particle time step.

III. RESULTS AND DISCUSSION

As shown in Fig. 3, we first examined spatial and temporal variations in the electrostatic potential within the trench by changing the trench width from 50 to 100 to 500 nm. The snapshots given here were selected to give an idea of the mean behavior ($\bar{X}$) and extremes ($\bar{X}\pm2\sigma$) for each trench size. To determine these values, we recorded potentials at all mesh points within the trench every 5000 ions/electrons until 1×10^7 ions/electrons entered the simulation domain, after an initial charge accumulation of 5×10^6 ions/electrons. These values were found sufficient to progress beyond the initial surface charging stage and capture meaningful statistics, as demonstrated in Fig. 4. Then, the average potential $\bar{V}$ of all locations within the trench was found for each set of recorded potentials. For 1000 sets of potential values (recorded from 5×10^6 to 1×10^7 ions/electrons entering the simulation domain for each trench width), the mean $\bar{X}$ and standard deviation σ of the potential averages were determined. The snapshots with average potentials $\bar{V}$ closest to $\bar{X}$ and $\bar{X}\pm2\sigma$ were then chosen as representative.

For the 500 nm width trench [Fig. 3(a)], a comparison among the potential contours reveals a lack of variability in the potentials, showing steady-state behavior. In each case, potentials of ~35 V are obtained near the trench exit, a significant barrier to low energy ions. In addition, the isolines are largely parallel to the x axis and somewhat equally spaced, indicating small x components and near-constant z components of the electric fields within the trench region.

The charging behavior changes dramatically as the trench dimension is decreased. By 100 nm [Fig. 3(b)], we see isolines with varying spacings and regions where they are no longer parallel to the x axis; the electric field components are no longer constant (E_z) nor insignificant (E_x). For extreme cases, the potential barrier at the exit has been reduced to ~10 V. A further decrease in size to 50 nm [Fig. 3(c)] results in a similar but more extreme behavior. Potentials range from −50 to 50 V, and the electric field strengths are larger, with E_z ranging from positive to negative along the centerline for the mean case. We can also surmise that the potential barrier within the trench is no longer a significant obstruction to low energy ions approximately half of the time.

While the contour plots clearly illustrate significant potential distribution changes with time as the trench width reduces below 100 nm, a more comprehensive look at the dimension effect is illustrated in Fig. 4. For larger trench widths, the potential slowly reaches a pseudo-steady-state with a relatively low standard deviation as the dielectric surfaces become charged. For the 500 nm wide trench [Fig. 4(a)], this buildup of charge on the bare surface occurs over

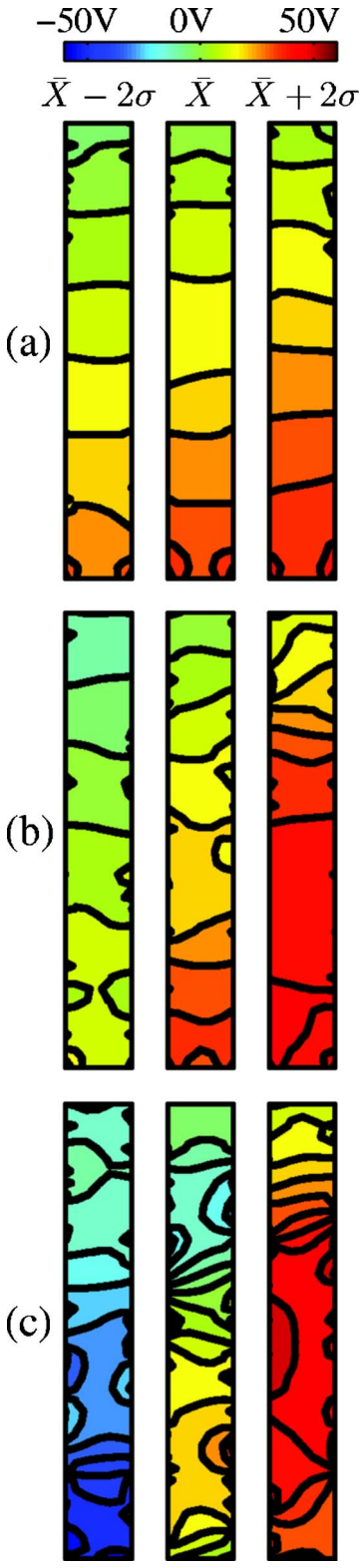

FIG. 3. (Color online) Potential contours within the trench, with snapshots indicating mean and mean ±2 standard deviations for (a) 500 nm wide trench, (b) 100 nm wide trench, and (c) 50 nm wide trench. The aspect ratio of all trenches is 5.

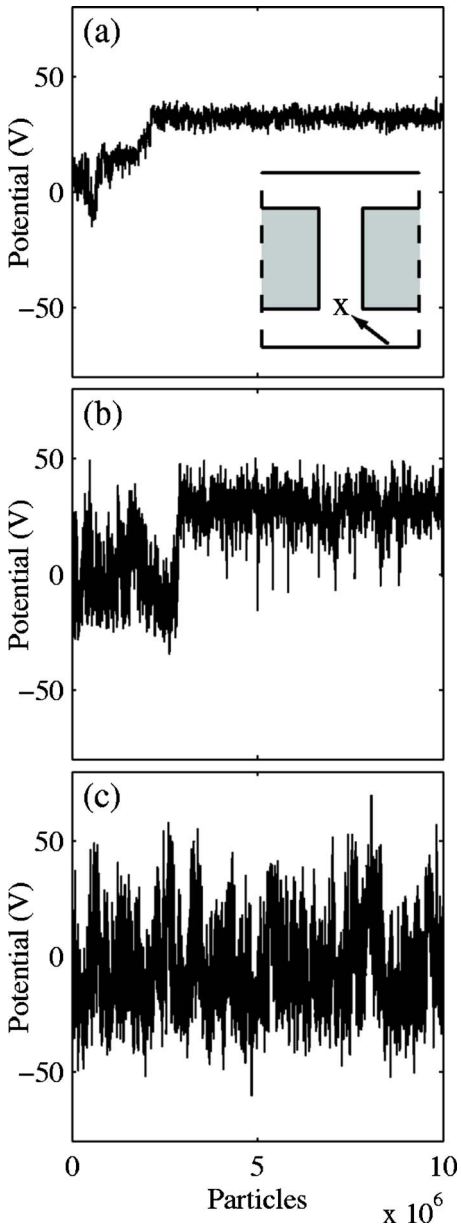

FIG. 4. (Color online) Variation of the potential with the number of combined ions and electrons entering the simulation domain for (a) 500 nm wide trench, (b) 100 nm wide trench, and (c) 50 nm wide trench. The aspect ratio of all trenches is 5. The inset indicates the position at which potential measurements are taken, the center of the bottom exit of the trench.

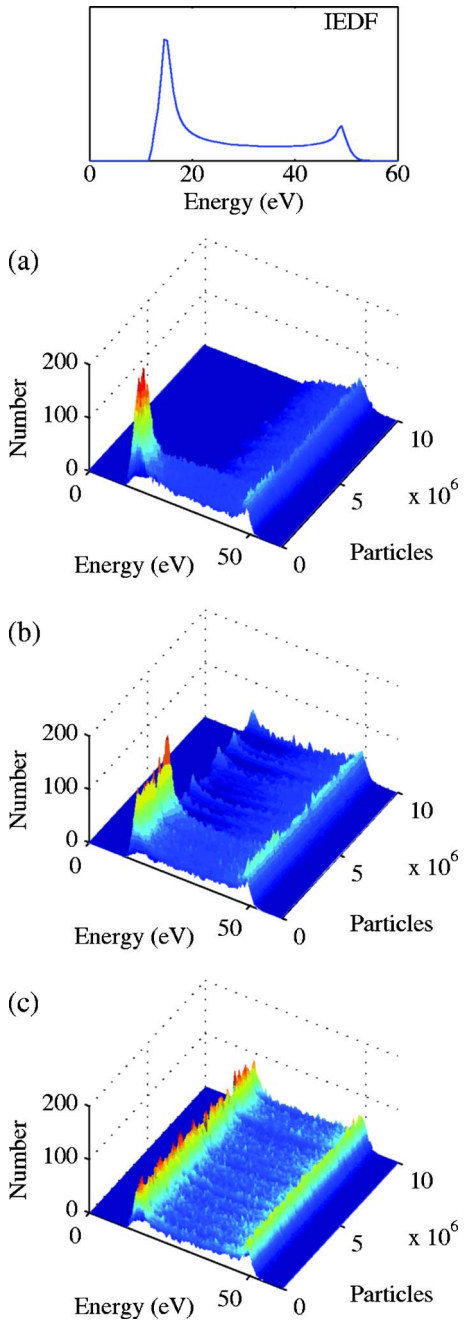

FIG. 5. (Color online) Extrusion plots showing numbers and energies of ions reaching the trench exit with the number of combined ions and electrons entering the simulation domain. (a) 500 nm wide trench. (b) 100 nm wide trench. (c) 50 nm wide trench. Intervals of 20 000 combined ions and electrons entering the domain are used between recording of data. The aspect ratio of all trenches is 5. Inset at top: Ion energy distribution function for ions entering the computational domain.

a period of roughly 2.5×10^6 combined ion and electron events. Under additional particle bombardment, the potential at the trench exit ranges from an average of ~32 V at the centerline to ~45 V near the sidewalls, with standard deviations of roughly 2.5 V.

This is in contrast with the behavior of a trench of width of 100 nm, as shown in Fig. 4(b). At this width, a near steady state is achieved after approximately 3×10^6 combined ions and electrons. After reaching this point, the mean potentials at the trench exit are comparable to those of the larger 500 nm wide trench, ranging from ~28 V at the centerline to ~40 V at the sidewalls. The standard deviations of these values are far larger, however, at ~8.5 and ~10.5 V at the centerline and sidewalls, respectively. Further, there are periodic spikes in these potentials wherein the potentials approach zero or become negative for short periods.

Below 100 nm, another type of behavior is observed, as illustrated by a 50 nm wide trench in Fig. 4(c). Here, no distinguishable region of charge buildup on the surface is observed; statistics on the potential at the trench exit are essentially unchanged whether taken starting from the first particle or after 5×10^6 particles have already bombarded the surface. The mean potentials are near zero or slightly negative at both the centerline and sidewalls, and the standard

deviations are ~22 and ~26 V, respectively. Thus the potential at the exit oscillates between being strongly positive and negative, with peaks of ±40 V. This clearly demonstrates that differential charging can show a stochastic behavior on nanopatterned dielectric surfaces, although subject to surface conductivity.

Next, as illustrated in Fig. 5, we looked at how the difference in the charging behavior influences the flux and the kinetic energy distribution of ions passing through the trench. The inset at the top shows the bimodal ion energy distribution function for ions entering the simulation domain, used for all dimensions considered. For the 500 nm wide trench, as demonstrated in Fig. 5(a), ions of all energies are able to pass through the trench during the initial surface charging stage. Once the pseudo-steady-state is reached, however, low energy ions entering the trench are either directed to the trench sidewall or forced out the trench entrance, as the potential barrier at the trench exit remains above 20 V at all times.

This situation changes for a trench of width of 100 nm, as indicated in Fig. 5(b). As with the larger trench described above, there is a period of charge buildup on the dielectric surface during which low energy ions may pass through the trench. Once the near steady state is reached, however, low energy ions are able to exit the trench on a periodic basis, corresponding to spikes wherein the potential in the trench is reduced to near or below zero.

As the trench width is reduced to 50 nm, low energy ions pass through the trench with little interruption throughout the duration of the simulation, as illustrated in Fig. 5(c). Again this can be explained through an investigation of the behavior of the potential. In this case, there is no discernible period of charge accumulation on the dielectric surface as seen with the larger trenches, so a relatively constant behavior of ion energies exiting the trench is expected. In addition, large fluctuations in the potential at the trench exit occur with high frequency, leading to roughly equal periods of the trench being positively and negatively charged and allowing a steady stream of low energy ions to pass through the trench.

IV. SUMMARY

We have investigated differential surface charging of high aspect ratio dielectric trenches under ion and electron bombardments using a two-dimensional computational model. Potential distributions in the computational domain were updated after charge transfer from each impinging ion or electron, with explicit treatment of the surface charge conduction. This approach allows us to track the fluctuations in potentials present within the trench region, unlike earlier methods which mostly looked at the steady-state charging behavior of patterned structures at the micron or larger scales, considering average fluxes of ions and electrons for a given period of time. Our results show an oscillation in the potential in high aspect ratio dielectric trenches, with both the magnitude and frequency of the oscillations increasing as the dimensions of the structure decrease. This effect is intertwined with the flux and energies of ions passing through the trench. Low energy species which were unable to reach the trench exit for a large trench width (500 nm) are able to pass through as structures shrink to 100 nm wide and below, with fluctuations mimicking the fluctuations in the potentials. While the two-dimensional model clearly demonstrates the possible occurrence of stochastic surface charging on high aspect ratio dielectric structures, our effort will be extended to three dimensions to note what effect, if any, the additional degree of freedom will have on this oscillating behavior, beyond perhaps a reduction in the absolute dimension at which the onset of the behaviors shown above occur. We expect the improved understanding of differential surface charging at the nanoscale will provide valuable guidance on applying plasma techniques to the fabrication of future nanostructure-based devices.

ACKNOWLEDGMENTS

The authors greatly acknowledge the National Science Foundation (CTS-0650536) and the Welch Foundation (F-1535) for their financial support.

[1] S. Iwata and A. Ishizaka, J. Appl. Phys. **79**, 6653 (1996).
[2] T. G. Northrop, Phys. Scr. **45**, 475 (1992).
[3] A. Barkan, N. Dangelo, and R. L. Merlino, Phys. Rev. Lett. **73**, 3093 (1994).
[4] H. B. Garrett, Rev. Geophys. **19**, 577 (1981).
[5] R. A. Gottscho, C. W. Jurgensen, and D. J. Vitkavage, J. Vac. Sci. Technol. B **10**, 2133 (1992).
[6] H. Shin, C. C. King, T. Horiuchi, and C. M. Hu, IEEE Electron Device Lett. **12**, 404 (1991).
[7] K. Hashimoto, Jpn. J. Appl. Phys., Part 1 **33**, 6013 (1994).
[8] G. S. Hwang and K. P. Giapis, J. Vac. Sci. Technol. B **15**, 70 (1997).
[9] J. C. Arnold and H. H. Sawin, J. Appl. Phys. **70**, 5314 (1991).
[10] D. J. Economou and R. C. Alkire, J. Electrochem. Soc. **135**, 941 (1988).
[11] T. Kinoshita, M. Hane, and J. P. McVittie, J. Vac. Sci. Technol. B **14**, 560 (1996).
[12] J. Matsui, K. Maeshige, and T. Makabe, J. Phys. D **34**, 2950 (2001).
[13] T. Tatsumi, Y. Hikosaka, S. Morishita, M. Matsui, and M. Sekine, J. Vac. Sci. Technol. A **17**, 1562 (1999).
[14] M. Matsumoto and T. Nishimura, ACM Trans. Model. Comput. Simul. **8**, 3 (1998).
[15] A. B. Birtles, J. Phys. D **5**, 1396 (1972).
[16] P. A. Heimann and J. E. Olsen, J. Appl. Phys. **53**, 546 (1982).